ORIGINAL PAPER

Propagation of highly nonlinear solitary waves in a curved granular chain

**Luyao Cai · Jinkyu Yang · Piervincenzo Rizzo ·
Xianglei Ni · Chiara Daraio**

Abstract We assemble granular chains composed of spheres of uniform diameter in different curved configurations. We study the properties of highly nonlinear solitary waves traveling in the curved channels as a function of the curve angle and of the radius of curvature, using experiments and numerical simulations. We observe that solitary waves propagate robustly even under drastic deflection, such as 90° and 180° turns. When the solitary waves encounter a sharp turn with a radius of curvature as small as one spherical particle's diameter, we report the formation of secondary solitary waves resulting from the interaction with the guiding rail. We compare experimental results with numerical simulations based on a discrete element model that accounts for nonlinear and dissipative interactions between particles. This study demonstrates that granular chains are efficient wave-guides, even in complex geometrical configurations. Moreover, the findings in this study suggest that solitary waves could be used as novel information and/or energy carriers.

L. Cai · P. Rizzo (✉) · X. Ni
Laboratory for Nondestructive Evaluation and Structural Health Monitoring Studies, Department of Civil and Environmental Engineering, University of Pittsburgh, 729 Benedum Hall, 3700 O'Hara St., Pittsburgh, PA 15261, USA
e-mail: pir3@pitt.edu

J. Yang
Department of Mechanical Engineering, University of South Carolina, 300 Main Street, Room A220, Columbia, SC 29208, USA

C. Daraio
Engineering and Applied Science, California Institute of Technology, 1200 E California Boulevard, MC 105-50, Pasadena, CA 91125, USA

C. Daraio
Department of Mechanical and Process Engineering, ETH Zürich, Tannenstrasse 3, 8092 Zürich, Switzerland

1 Introduction

Over the last decade, the study of highly nonlinear solitary waves (HNSWs) has drawn increasing attention at the fundamental level and for engineering applications [1–30]. HNSWs can be generated in a straight chain of spherical particles, where dispersive and nonlinear effects, due to the discreteness of the system and the Hertzian contact among spheres, are balanced. We refer to such ordered granular chains as one-dimensional (1D) granular crystals. Previous studies suggested HNSWs for different engineering applications, for example, as impurity detectors in granular systems [3,7], nozzle-free ink-jet printer [5], acoustic lenses [20], impact mitigation [8,13,18], and nondestructive testing [17,26–30]. In these applications, the granular crystals serve as a new type of waveguide and/or information carrier by transmitting, redirecting, or blocking solitary waves in a controllable and efficient manner.

Previous studies mainly focused on the propagation of solitary waves in a "straight" 1-D array of particles. The physical mechanism of solitary waves' transmission in "deflected" or "curved" chains is largely unexplored. Daraio et al. [19] have reported flexible redirecting and splitting of solitary waves in a straight granular chain that diverges into two branches using Y-shaped guides. Yang et al. [25] studied the propagation of solitary waves in a curved granular crystal enclosed by flexible guides with the focus on the coupling between the granules and the deformable media for impact mitigation. However, no studies systematically characterized the effects of chain deflection and radius of curvature on the solitary waves' transmission and reflection.

In this study, we investigated experimentally and numerically how the characteristics of solitary waves are affected by the geometry of a bent granular chain. Particularly, we evaluated the effect of the radius of curvature and the deflection angle between two straight granular segments on the transmission efficiency of the waves. For the experimental study, we connected two straight granular segments supported by modular guiding rails that could be configured in different curvatures and deflection angles. We measured the waves' characteristics using sensors located before and after the curved section of the chain. The results were compared with numerical simulations based on a discrete element model (DEM) that accounted for nonlinear and dissipative effects in the particles' interactions. We found that solitary waves can be efficiently transmitted in a curved chain through the point contact between grains, maintaining their compact shape. Particularly, even under drastic bends, such as 90° and 180° turns, the solitary waves preserved a significant portion of the momentum and energy. This suggests the use of granular chains as flexible wave-guides for momentum and energy transmission of elastic waves. If the granular chains exhibit sharp turns, with radii of curvatures as small as a one spherical particle's diameter, we observed that the solitary waves are partially transmitted across the bends and secondary reflected solitary pulses are formed.

The paper is organized as follows: In Sect. 2, we describe the experimental setup. In Sect. 3, we introduce the DEM used to simulate the propagation of solitary waves in the curved chains. The experimental and numerical results are discussed in Sect. 4. We conclude the paper in Sect. 5 with a summary of findings and their implications.

2 Experimental setup

To evaluate the effect of the granular chain's geometry on the propagation of HNSWs, we assembled modular guide rails in a variety of configurations. Each configuration was built by connecting two straight channels with curved rails, which had different radii of curvature and bent angles. Figure 1a displays one of the configurations used to evaluate the effect of the angle θ at a constant radius of curvature R_c. The front and rear straight chains were composed of $N_1 = 18$ and $N_3 = 15$ spheres, respectively, confined by structural fiberglass square tubes (having sides 25.4×25.4 mm, and wall thickness 3.175 mm, McMaster–Carr product number 8548K21), with the first particle being the striker bead. The curved channels were made of Delrin acetal resin to reduce friction. The elastic modulus and Poisson's ratio of the Delrin guide were $E_G = 3.2$ GPa and $v_G = 0.35$, respectively. The particles were stainless steel bearing-quality balls (type 302, McMaster–Carr) with a diameter $D = 19.05$ mm, mass $m = 29$ g, elastic modulus $E = 200$ GPa, and Poisson's ratio

$v = 0.28$. The number of particles (N_2) in the curved section was varied depending on the bent angle and the curvature.

We conducted two sets of experiments. In the first set, we investigated the effect of the deflection angle θ on the amplitude of the propagating solitary waves. We considered nine different angles ($\theta = [0°, 30°, 45°, 60°, 90°, 120°, 135°, 150°, 180°]$) keeping the radius of curvature constant and equal to $R_c = 76.20$ mm. The photo of the setup is shown in Fig. 1a with the different elbows presented in the inset. These angles tested correspond to $N_2 = [1, 3, 3, 5, 7, 9, 9, 11, 13]$ included in the curved rail. To ensure the contact between adjacent particles, the whole system leaned against a reaction wall mounted at the end of the third segment.

In the second set of experiments, we systematically varied R_c in order to evaluate the effect of the chain's curvature on the solitary wave's properties. We devised six different segments that deflected the direction of the wave propagation by 90°. We considered R_c equal to $19.05 \times [1, 2, 3, 4, 5, 6]$ mm. Figure 1b displays the setup and the different bent sections used. The corresponding number N_2 of beads along the curve was equal to $N_2 = [1, 3, 5, 7, 7, 9]$. The bent section with the largest radius of curvature ($R_c = 6d$) hosted nine spheres, while the smallest ($R_c = d$) contained only a single particle.

For both sets of experiments, the solitary waves were excited by the transducer shown in Fig. 2a. It consisted of an electromagnet made of a magnetic wire coil (AWG24) of about 1,350 turns wrapped around a 13 mm diameter and 33 mm long iron core. The electromagnet lifted a striker particle (19.05 mm-diameter) along the plastic slider. A DC power supply (BK precision Model 1672) was used to provide electrical current to the coil. The drop height of the striker was 4.7 mm, resulting in the striker velocity $v \sim 0.30$ m/s. To prevent the movement of the first particle of the chain toward the slider, a small plastic sleeve was glued to the bottom of the electromagnet. As the electrical resistance of the coil depends on the coil temperature, the power supply was used in current control mode to keep the current constant. The electromagnet was coupled to a switch circuit, driven by a National Instruments—PXI running in LabVIEW. With the switch closed, the electrical current passed through the coil allowing the motion of the striker. A LabVIEW front panel was designed to operate the actuator automatically.

Five sensor particles were assembled and used to measure the propagation of the HNSWs generated by the mechanical impact of the striker. Each sensor bead contained a piezoelectric ceramic disc (circular plate with 0.3 mm thickness and 19.05 mm diameter) with silver electrodes and microminiature wiring (Fig. 2b). The assembling and calibration procedures of the instrumented particles were similar to those described in [12]. To quantify the effect of the geometry on the properties of the solitary waves, two sensor beads, namely S_1 and S_2, were positioned along the first segment at the 11th and 16th positions (see Fig. 1). These sensors measured the

Fig. 1 Digital images of the experimental setups. **a** Setup to study the effect of variable deflection angles θ at a given radius of curvature R_c. The setup presented in the photo has $\theta = 120°$ and a radius of curvature $R_c = 4d$ (bead diameter $d = 19.05$ mm). The *inset* shows an assortment of eight different curved guide rails with $\theta = [30°, 45°, 60°, 90°, 120°, 135°, 150°, 180°]$ and $R_c = 4d$. **b** Setup to study the effect of different radii of curvature at a given deflection angle. The setup presented in the photo has $\theta = 90°$ and $R_c = d$ (bead diameter $d = 19.05$ mm). The *inset* shows an assortment of six different guide rails with a right angle and $R_c = [1, 2, 3, 4, 5, 6] \times d$
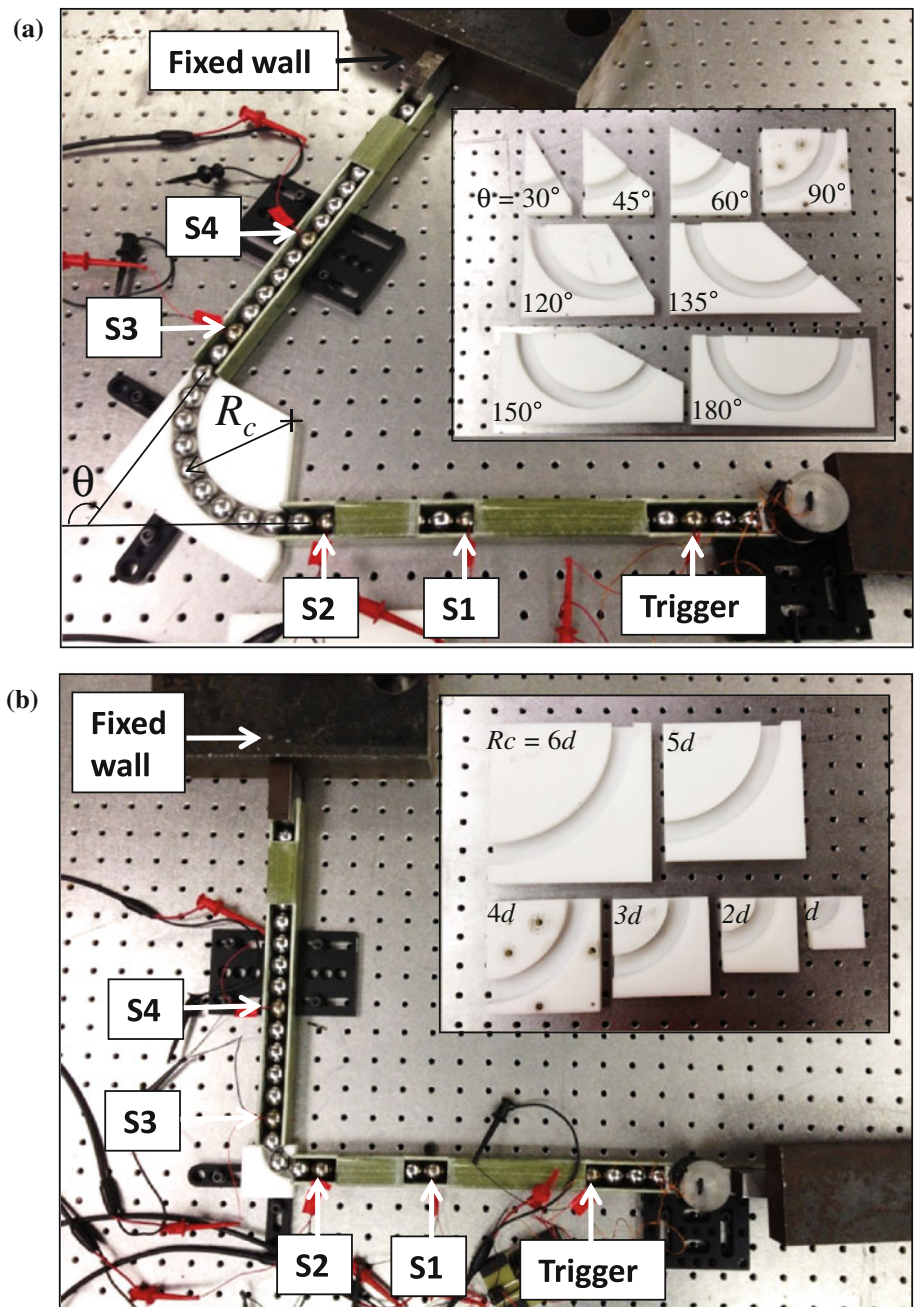

Fig. 2 **a** Photo of the electromagnet employed to lift the striker particle along a plastic slider. **b** Schematic of a PZT-embedded sensor particle used for capturing the propagation of solitary waves
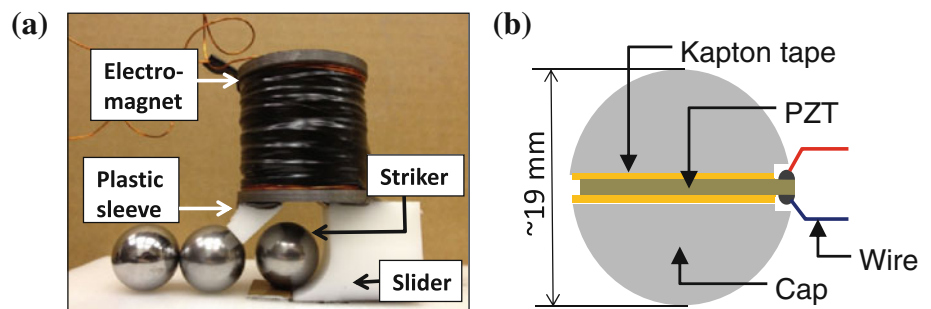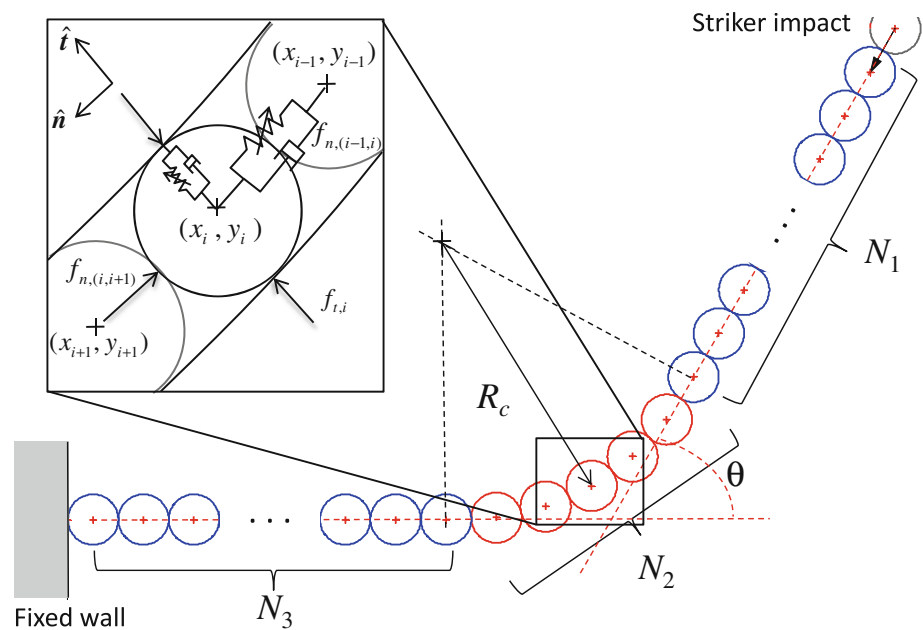
Fig. 3 Schematic diagram of the 2D DEM. θ is the deflection angle and R_c the radius of curvature. The number of spherical particles in the curved section (N_2) is determined by θ and R_c and it is summarized in Table 1. The *inset* shows the approximation of spherical particles into point-masses connected by nonlinear springs and dampers

characteristics of the solitary waves before they reach the elbow. Two sensors, S_3 and S_4, were positioned along the 2nd and 7th positions of the straight segment after the bend in order to capture the waveforms and to measure the wave's speed after the elbow. The sensor particles were connected to an oscilloscope and the signals were digitized at 10 MHz sampling rate. To assess repeatability, 50 measurements were taken for each case and processed statistically in Matlab.

3 Numerical approach

We simulated the propagation of solitary waves in granular crystals using a DEM [1,25]. The DEM approach approximated the granular chain as an assembly of discrete lumped masses connected by interfacial springs, similar to a molecular dynamics approach. In this study, we accounted for the nonlinear and dissipative nature of the particles' axial interactions to predict the attenuation of the traveling waves. Tangential interactions were neglected, assuming that the rotational motion of the particles was very small. We will later discuss the validity of this assumption based on the numerical results.

Figure 3 illustrates a schematic diagram of the DEM model, including the deflection angle θ and the radius of curvature R_c. The contact force $\boldsymbol{f_n}$ between two neighboring particles can be described as:

$$\boldsymbol{f_n} = \left[A_n \delta_n^{3/2} + \gamma_n \dot{\delta}_n \right] \hat{\boldsymbol{n}}, \tag{1}$$

where δ_n is the approach under the compressive interactions and $\hat{\boldsymbol{n}}$ is the unit vector in the direction of their center-

of-mass alignment. The first term represents the nonlinear Hertzian contact force between two identical spherical bodies. According to the Hertzian contact law, the contact coefficient A_n can be expressed as $E\sqrt{D}/[3(1-v^2)]$ with E, v, and D denoting elastic modulus, Poisson's ratio, and diameter of the spherical particles, respectively [31]. The dissipative effect caused by damping factors, such as friction and viscoelasticity, is taken into account by the second term, which is based on the damping model developed by Tsuji et al. [32]. In this model, the damping coefficient γ_n is given by:

$$\gamma_n = \alpha_n (m A_n/2)^{1/2} \delta_n^{1/4}. \tag{2}$$

Here, m is the particle mass and α_n is the constant that can be analytically deduced from the coefficient of restitution (e) between two colliding identical particles [32], which is defined as the ratio of the rebounding particle velocity to the incident one under collision. However, the dynamics of the granular chain in this study involves multiple particle interactions [1]. As a consequence, the analytical value α_n obtained for a two-particle collision does not accurately account for the chain's dissipation. We empirically determined the axial dissipation coefficient $\alpha_n = 0.02$ to match experimental results. This value falls in the range $a_n = 0.01$–0.05 predicted analytically by the Tsuji's model [32]. According to the Tsuji's analytical relationship between e and α_n, this corresponds to $e \approx 0.95$ and matches reasonably well the experimentally reported restitution coefficients of stainless steel spheres [33,34].

In this study, the elastic contact relationship between the granules and the guiding walls was built based on the Hertzian contact law similar to the axial relationship [31].

As shown in Fig. 3, transverse forces arise when the granules are confined in a curved section. The net force by the misaligned axial compressions is balanced with the normal force by the wall. The transverse contact force f_t against the guide can be expressed as:

$$f_t = \left[A_t \delta_t^{3/2} + \gamma_t \dot{\delta_t} \right] \hat{t}, \tag{3}$$

where δ_t is the sphere's displacement in the transverse direction $\hat{t}$ (Fig. 3). Note that the direction of the transversal contact force can be either inward or outward, depending on which rail the sphere forms contact with. In Eq. (3), the contact coefficient is:

$$A_t = \frac{2\sqrt{2D}}{3\left[\frac{1-\nu^2}{E} + \frac{1-\nu_G^2}{E_G} \right]}, \tag{4}$$

where E_G is the wall's elastic modulus and ν_G the wall's Poisson's ratio [31]. The damping coefficient γ_t takes a modified form compared to (2) as [25,32]:

$$\gamma_t = \alpha_t (m\, A_t)^{1/2} \delta_t^{1/4}. \tag{5}$$

The damping parameter $\alpha_t = 0.999$ was selected empirically to match the experimental results, as presented in Sect. 4. Note that this damping parameter in the transverse direction is much larger than α_n that we obtained for the axial damping. This is because the interactions of stainless-steel particles with the Delrin guide are more dissipative compared to the particle-to-particle interactions due to the viscoelastic effect of the polymeric wall.

Based on the contact forces exerted on the spheres, we built the equation of motion for the ith particle:

$$a_i = \frac{\sum \left(f_{n,(i-1,i)} + f_{n,(i,i+1)} + f_{t,i} \right)}{m}, \tag{6}$$

where a_i is the acceleration (see Fig. 3 for the notations of force components). We solve this differential equation to calculate each particle's displacements using a Runge–Kutta-4 integration scheme in Matlab.

4 Results and discussion

4.1 Effect of the deflection angle

Figure 4 shows the temporal force profile measured by the four sensor particles, normalized with respect to the force magnitude (A_{S1}) measured by the first sensor S_1, when $q = 0°$. The experimental results (presented with solid lines) are superimposed to the numerical results (presented with dotted lines). The profiles are shifted vertically to ease visualization. We observe the formation of a single compactly supported pulse. We find that the amount of attenuation of this incident solitary wave is not significant, as suggested by the
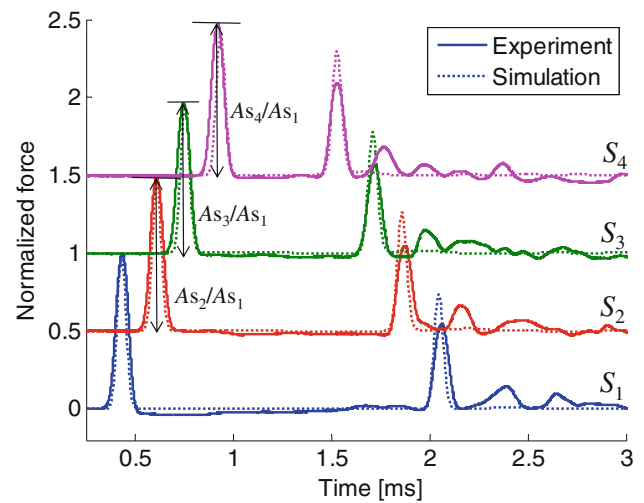

Fig. 4 Temporal force profiles of solitary waves propagating along a straight granular chain ($\theta = 0°$). Each force profile recorded from one of four sensors (S_1, S_2, S_3, and S_4) was normalized with respect to the maximum force magnitude of S_1 measurement (denoted as As_1), and is shifted vertically by 0.5 to ease visualization. Experimental and numerical results are represented by *solid* and *dotted curves*, respectively

ratios of the peak amplitude measured by the different sensors with respect to that measured by sensor S_1 ($A_{s2}/A_{s1} = 0.984$, $A_{s3}/A_{s1} = 0.964$, and $A_{s4}/A_{s1} = 0.975$). The solitary wave reflects from the hard wall positioned at the end of the rear segment, and it is again measured by the sensors as shown by the second pulse in each profile. The reflected pulse is followed by a smaller pulse which denotes secondary solitary waves, probably generated during the interaction with the wall at the end of the chain. The forming mechanisms of such secondary solitary pulses will be briefly discussed in Sect. 4.2, while the details can be found in [24]. We find that the overall shape of the propagating pulses is identical throughout the chain, and the experimental and numerical results are in very good agreement. The noticeable attenuation of the reflected solitary waves is due to losses at the end wall.

The transmission of solitary waves through a 90°-curved chain is illustrated in Fig. 5, which refers to $R_c = 6d$, where $d = 19.05$ mm is the bead diameter. Compared to the straight chain, we clearly observe the attenuation of solitary waves in the signals measured from S_3 and S_4 after the curved section. The normalized peak amplitude of sensors S_3 and S_4 are $As_3/As_1 = 0.723$ and $As_4/As_1 = 0.722$, respectively. Thus, it is evident that the presence of the 90° elbow mostly contributes to the decrease of the amplitude of the traveling wave. This is due to the loss of force components to the guiding rail through the lateral contacts in the curved section. A small fraction of the force loss is due to the presence of five more particles (when compared to the 0° case) between sensors S_2 and S_3. Despite the reduction in the force ampli-
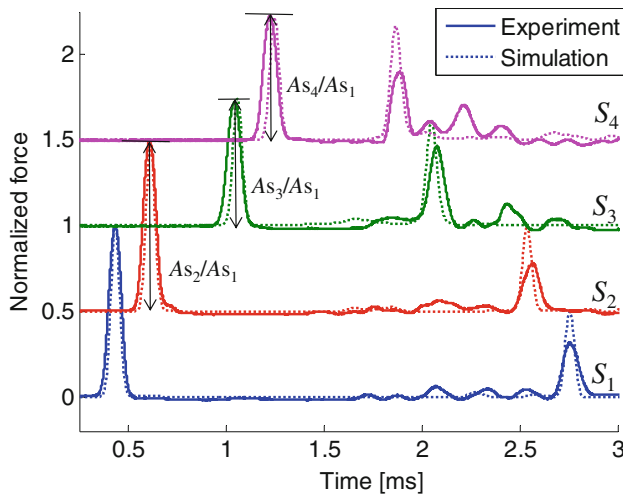
Fig. 5 Temporal force profiles of solitary waves propagating along a curved granular chain with $\theta = 90°$ and $R_c = 6 \times d$. We find that the amplitude of the solitary wave traveling after the curved section, measured by sensor beads S_3 and S_4 is attenuated noticeably. This is different from the conservative trend of solitary wave propagation in a straight chain as shown in Fig. 4

Fig. 6 Transmission ratios of solitary waves through curved segments as a function of the deflection angles θ. The discrete points with *error bars* (95 % CI) represent the experimental values, while *lines* denote numerical results obtained from DEM

tude, we observe that the shape of the incident wave is preserved remarkably well after the bend, as shown in S_3 and S_4 signals around 1.0 and 1.2 ms-time. Moreover, there are negligible reflections generated by the elbow. Thus, the granular chains can efficiently transmit solitary waves without significant distortion even in a sharp turn such as 90°.

The transmission ratio of the solitary waves before and after the bent section was quantified for all nine deflection angles considered. Figure 6 shows the transmission ratio A_{Sn}/A_{S1} ($n = 2, 3, 4$) as a function of the angle θ. Each dot indicates the average value of the 50 measurements taken at each angle, and the vertical error bars denote a 95.5 % (2σ) confidence interval (CI). The barely visible error bars demonstrate the repeatability of the testing. Figure 6 shows that the amplitude of the solitary waves linearly decreases with the increase of the deflection angle. Notably, when the solitary wave is redirected by 90°, the transmission ratio is 0.65. At 180°-turn, 47 % of the solitary wave's amplitude is transmitted to the rear straight segment. These experimental values are superimposed to the numerical results obtained using the DEM described in Sect. 3. We find that the numerical and experimental results are in excellent agreement. Note that rotational mechanics of granules was not taken into account in the DEM model. This means that the primary mode of energy and momentum transmission in 1D granular chains is through axial contacts. Thus, the capability to transmit the wave along the chain is attributed to the axial "point" contact between granules, which leads to the formation of robust solitary waves. This is in contrast to random, dissipative granular architectures in which particles' rotational dynamics cannot be neglected.
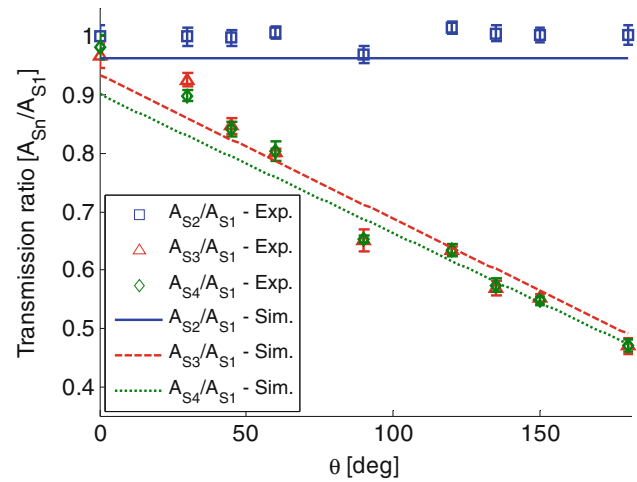
The velocities of the solitary pulse before and after the curved segment are reported in Fig. 7 as a function of the deflection angle. Experimentally, we observe a linear decrease of the speed. At 180°, the speed of transmitted solitary wave is about 13 % lower than that of the straight chain. The general trend of the velocity curve is very similar to that of the transmission ratio in Fig. 6. This is due to the unique nature of nonlinear waves that exhibit strong dependence of wave speed on its amplitude. In the case of highly nonlinear solitary waves, the wave's propagation speed, v_s, is related to the wave's maximum amplitude, F_m, as $v_s \sim F_m^{1/6}$ [1,16]. In Fig. 7, we notice some discrepancies between the experimental and numerical results, though their responses are qualitatively similar. Such discrepancies might be caused by the inaccurate simulation parameters, such as striker velocity and material properties, or by more complex dissipative effects in experiments than those accounted for in the numerical model.

4.2 Effect of the curvature

As summarized in Table 1, we studied six different radii of curvature (R_c) that deflected the trajectory of the wave propagation direction by 90°. The numerical and experimental normalized force profiles for the smallest R_c are presented in Fig. 8. The amplitude of the traveling pulse measured by sensor S_2 is 99.2 % of the amplitude measured by the first sensor, i.e. $A_{S2}/A_{S1} = 0.992$, and the wave maintains its robust, single-hump shape. However, we witness significant attenuation of solitary waves after the bent section. The relative amplitudes of the solitary waves' peaks were 0.390 and 0.384, respectively, when measured from S_3 and S_4. This is a higher attenuation compared to the 90°-deflection with a larger radius of curvature ($R_c = 6d$).
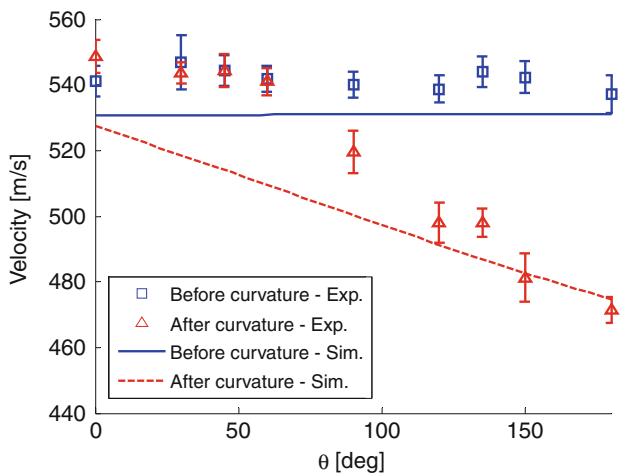
Fig. 7 Velocities of solitary waves as a function of deflection angles θ, measured before (*solid*) and after (*dashed*) deflection. The discrete points with *error bars* (95 % CI) represent the experimental values, while *lines* denote numerical results obtained from DEM

Fig. 8 Temporal force profiles of solitary waves propagating along a curved granular chain with $\theta = 90°$ and $R_c = d$. Compared to the results from a larger curvature (e.g., $R_c = 6 \times d$ in Fig. 5), we find that the solitary waves are further attenuated after the deflection. The presence of secondary solitary waves generated by the elbow is emphasized with *dashed circles*

Table 1 Geometric properties of the curved granular chains investigated in this study

Experiment	N_1	N_2	N_3	q (°)	R_c (mm)
Set 1: effect of the deflection angle	18	1	15	0	76.20
	18	3	15	30	76.20
	18	3	15	45	76.20
	18	5	15	60	76.20
	18	7	15	90	76.20
	18	9	15	120	76.20
	18	9	15	135	76.20
	18	11	15	150	76.20
	18	13	15	180	76.20
Set 2: effect of the radius of curvature	18	1	15	90	19.05
	18	3	15	90	38.10
	18	5	15	90	57.15
	18	7	15	90	76.20
	18	7	15	90	95.25
	18	9	15	90	114.3

Besides the reduction in the force amplitude, the small radius of curvature induces the formation of secondary solitary waves even before the reflection from the wall, as indicated by the circles in Fig. 8. These secondary waves tail the incident pulse and are partially transmitted and partially reflected at the elbow. According to previous studies, the mechanism of formation of secondary solitary waves can be explained by the complex dynamic interaction between the particles and their bounding media [10,24]. When a granule collides against a "soft" wall, its contact time tends to be significantly longer, due to the low contact stiffness at
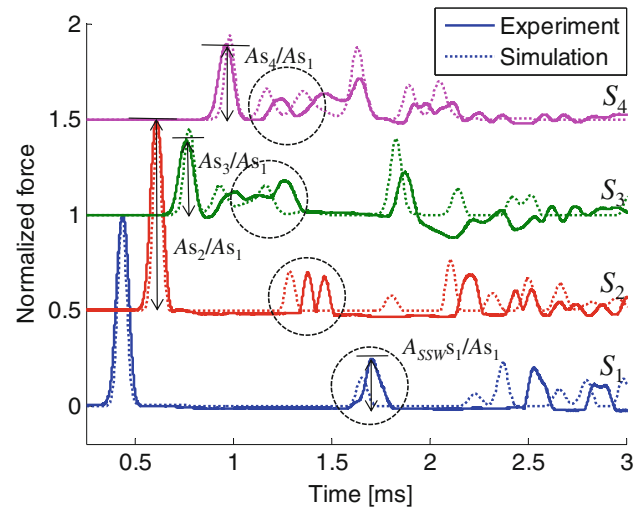
the wall interface. This causes the separation of the particle from the rest of the chain. Eventually, the rebounding particle against the wall collides with the chain, resulting in the partial reflection of incoming solitary waves. At the same time, the transmitted solitary waves experience the disintegration into a group of primary and secondary solitary waves due to the multiple collisions among the granules. The details of such complex particle dynamics in relation to material properties are described in the reference [24].

In the bent chains tested in this study, the propagation of solitary waves is obstructed by the guiding structure. The momentum carried by the incident wave is split between the transmitted pulse and a secondary reflected solitary pulse, and it is also partially dispersed to the guiding material. If the curvature is low (i.e. if the radius of curvature is high), the interaction between the spheres and the rail is not significant, and no secondary pulses are formed (for example, when $Rc = 6d$). We found experimentally that the mechanism of formation of secondary waves at the elbow is not only affected by the chain curvature, but also by the deflection angle and the combination of spheres' and rail's material properties. According to the findings in [24], we speculate that the softer the guiding rail is, the more likely is the secondary solitary wave's formation.

We numerically calculated the ratios of secondary solitary waves' amplitude (A_{SSW}, s_1) to those of the incident waves (A_{s1}) based on the S_1 signals from a 90°-bend chain (see Fig. 8). The results are shown in Fig. 9. As predicted, we observe larger magnitudes of secondary solitary waves for the granular chains with smaller radii of curvature. The sudden
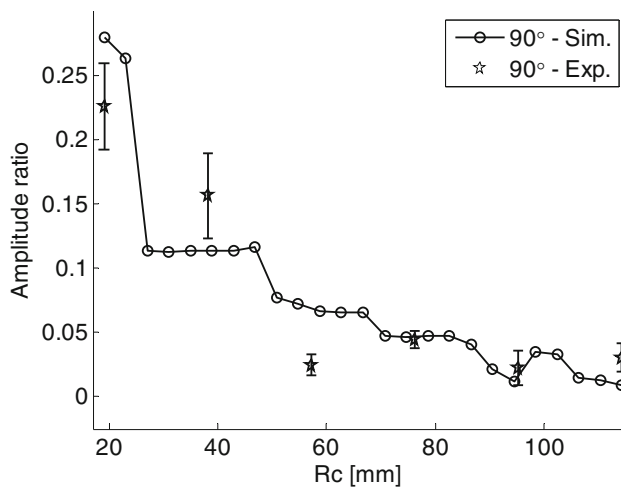
Fig. 9 Amplitude ratios of secondary solitary waves relative to those of incident solitary waves. The *circular dots* connected with a *solid line* represent simulation results, while *star marks* with *error bars* denote experimental data, all viewed from the sensor S_1

Fig. 10 Transmission ratios of solitary waves through curved segments as a function of the radius of curvature R_c. The discrete points with *error bars* (95 % CI) represent the experimental values, while *lines* denote numerical results obtained from DEM

Fig. 11 Velocities of solitary waves as a function of the radius of curvature R_c. The discrete points with *error bars* (95 % CI) represent the experimental values, while *lines* denote numerical results obtained from DEM

drops in the curves are caused by the discrete change of particle numbers in the curved section. Experimental data, marked in stars, follow the trend qualitatively. We also performed numerical simulations for other angles, and we found that the magnitudes of secondary solitary waves tend to increase as the deflection angle changes from 0° to 90°. However, beyond the 90° bend, there was no clear correlation between secondary solitary waves' amplitudes and the deflection angles.

Figure 10 reports the transmission efficiency of solitary waves as a function of the radius of curvature. The amplitude of the pulse prior to the bend is almost one, showing negligible dissipation of the pulses in the straight segments, between the sensors S_1 and S_2. However, the amplitude of the pulse after the bend is reduced as the radius of curvature becomes smaller. We find that the experimental results (represented by the dots in Fig. 10) match reasonably well the numerical results (represented by the curves). The noticeable discrepancy evident in the results obtained for the small radii of curvature might be originated from the tangential interactions of the particles in experiments, which were neglected in our numerical DEM approach. The velocities of the solitary waves before and after the various curvatures are plotted in Fig. 11. For the chains with the larger curvatures (i.e., a sharp 90°-turn), we observe more reduction of the transmitted solitary waves' speed. Again, such decrease in speed is attributed to the attenuation of solitary waves due to the interaction with the curved mechanical channels.

The summary of the transmission efficiency as a function of the varying radius of curvature, R_c, and deflection angle, θ, included in our study is plotted in Fig. 12. The results are based on the simulated force profiles of the S_3 signals obtained from the DEM. We observe the gradual reduction
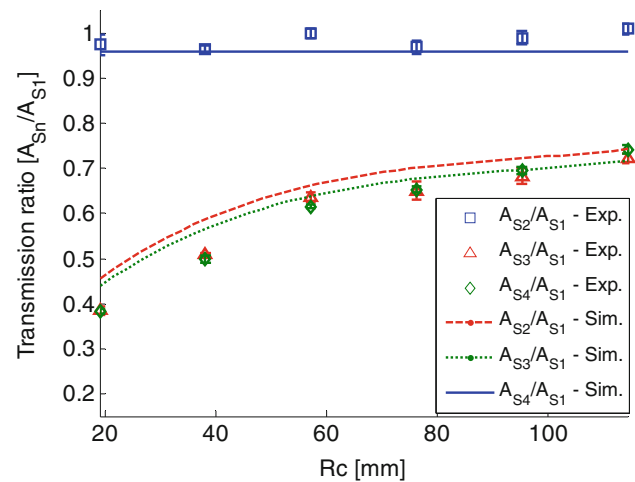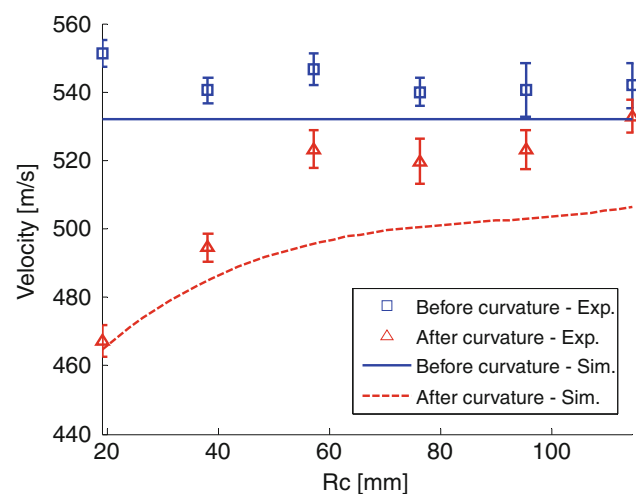
of solitary wave transmission ratios as the deflection angle increases or the radius of curvature decreases. It is evident that a granular chain with a modest curvature (e.g., $R_c > 3d$, where d is a particle diameter) can successfully transmit incident solitary waves with a more than 50 % of transmission ratios, even under the drastic deflection angles such as 90° and 180°. Such flexibility of wave transmission can be exploited for employing granular crystals as novel momentum and energy transmission channels.
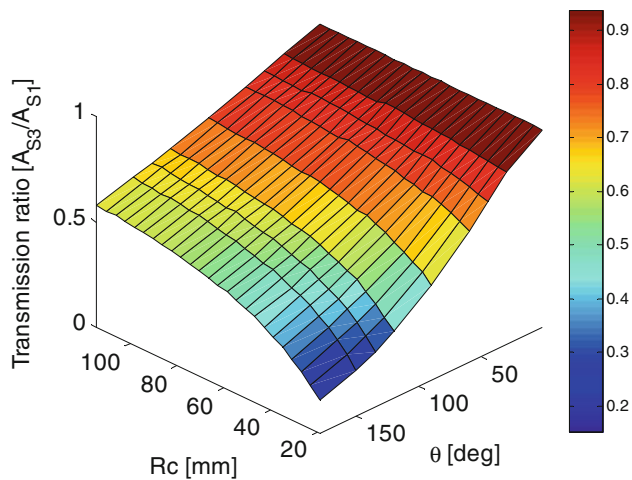
Fig. 12 Surface map of solitary waves' transmission ratios as a function of deflection angle θ and radius of curvature R_c. The results are based on the simulated results of S_3 signals obtained from DEM

5 Conclusions

In this paper, we investigated the propagation of highly nonlinear solitary waves in a curved chain composed of spherical particles. We characterized the effect of the bend's geometry on the amplitude and speed of the propagating waves. We systematically varied the deflection angle and the radius of curvature between two straight chains. Experimental results were compared to numerical results based on a DEM, which included dissipative losses in the axial interactions. We found that the attenuation of solitary waves is highly dependent on the chain deflection angles and curvatures. Notably, as a single pulse propagates through the bent chain, 71 % of its initial force amplitude is preserved even under the 90° turn, and 50 % of its force amplitude is preserved after a 180° turn. We also observed the formation of secondary solitary waves in the chains with a sharp turn (i.e., a small radius of curvature) that are caused by interactions with the guiding rails.

The measured transmission ratios for the curvatures tested were in the range of 40–70 %, implying noticeable loss of energy through the bent chains. However, it should be noted that for a radius of curvature larger than approximately three times of the particle diameters, the original shape of a solitary pulse is well preserved without being disintegrated into a group of solitary waves. Thus, despite the loss of energy, such bent chains can serve as an information transmission line for engineering applications.

The findings in this study can be useful when granular chains are employed as wave guides for example in actuators and sensors for the nondestructive evaluation of structural and biological materials. We limited our work to the investigation of chain geometry effects in terms of curvatures and deflection angles. Further studies can be performed to pro-

vide a predictive tool to assess the behavior of HNSWs under various combinations of particles' dimensions and guiding rail's materials.

References

1. Nesterenko, V.F.: Dynamics of Heterogeneous Materials. Springer, New York (2001)
2. Coste, C., Falcon, E., Fauve, S.: Solitary waves in a chain of beads under Hertz contact. Phys. Rev. E **56**, 6104–6117 (1997)
3. Sen, S., Manciu, M., Wright, J.D.: Solitonlike pulses in perturbed and driven Hertzian chains and their possible applications in detecting buried impurities. Phys. Rev. E **57**(2), 2386–2397 (1998)
4. Chatterjee, A.: Asymptotic solution for solitary waves in a chain of elastic spheres. Phys. Rev. E **59**, 5912–5919 (1999)
5. Sen, S., Manciu, M., Manciu, F.S.: Ejection of ferrofluid grains using nonlinear acoustic impulses—a particle dynamical study. Appl. Phys. Lett. **75**, 1479–1481 (1999)
6. Manciu, F.S., Sen, S.: Secondary solitary wave formation in systems with generalized Hertz interactions. Phys. Rev. E **66**(1), 016616-1–016616-11 (2002)
7. Hong, J., Xu, A.: Nondestructive identification of impurities in granular medium. Appl. Phys. Lett. **81**, 4868–4870 (2002)
8. Hong, J.: Universal power-law decay of the impulse energy in granular protectors. Phys. Rev. Lett. **94**(10), 108001-1–108001-4 (2005)
9. Vergara, L.: Scattering of solitary waves from interfaces in granular media. Phys. Rev. Lett. **95**, 108002-1–108002-4 (2005)
10. Job, S., Melo, F., Sokolow, A., Sen, S.: How Hertzian solitary waves interact with boundaries in a 1D granular medium. Phys. Rev. Lett. **94**(17), 178002-1–178002-4 (2005)
11. Nesterenko, V.F., Daraio, C., Herbold, E.B., Jin, S.: Anomalous wave reflection at the interface of two strongly nonlinear granular media. Phys. Rev. Lett. **95**, 158702-1–158702-4 (2005)
12. Daraio, C., Nesterenko, V.F., Herbold, E.B., Jin, S.: Strongly nonlinear waves in a chain of Teflon beads. Phys. Rev. E **72**(1), 016603-1–016603-9 (2005)
13. Daraio, C., Nesterenko, V.F., Herbold, E.B., Jin, S.: Energy trapping and shock disintegration in a composite granular medium. Phys. Rev. Lett. **96**(5), 058002-1–058002-4 (2006)
14. Rosas, A., Romero, A.H., Nesterenko, V.F., Lindenberg, K.: Observation of two-wave structure in strongly nonlinear dissipative granular chains. Phys. Rev. Lett. **98**, 164301-1–164301-4 (2007)
15. Job, S., Melo, F., Sokolow, A., Sen, S.: Solitary wave trains in granular chains: experiments, theory and simulations. Granul. Matter **10**, 13–20 (2007)
16. Sen, S., Hong, J., Bang, J., Avalos, E., Doney, R.: Solitary waves in the granular chain. Phys. Rep. **462**(2), 21–66 (2008)
17. Khatri, D., Rizzo, P., Daraio, C.: Highly nonlinear waves' sensor technology for highway infrastructures. In: SPIE Smart Structures/NDE, 15th Annual International Symposium. San Diego, CA, Manuscript number 6934-25 (2008)
18. Fraternali, F., Porter, M.A., Daraio, C.: Optimal design of composite granular protectors. Mech. Adv. Mater. Struct. **17**, 1–19 (2009)

19. Daraio, C., Ngo, D., Nesterenko, V.F., Fraternali, F.: Highly nonlinear pulse splitting and recombination in a two-dimensional granular network. Phys. Rev. E **82**(3), 036603-1–036603-8 (2010)

20. Spadoni, A., Daraio, C.: Generation and control of sound bullets with a nonlinear acoustic lens. Proc. Natl. Acad. Sci. U.S.A. **107**(16), 7230–7234 (2010)

21. Ni, X., Cai, L., Rizzo, P.: A comparative study on three different transducers for the measurements of nonlinear solitary waves. Sensors **13**(1), 1231–1246 (2013) (special issue)

22. Santibanez, F., Munoz, R., Caussarieu, A., Job, S., Melo, F.: Experimental evidence of solitary wave interaction in Hertzian chains. Phys. Rev. E **84**, 026604-1–026604-5 (2011)

23. Ni, X., Rizzo, P., Daraio, C.: Actuators for the generation of highly nonlinear solitary waves. Rev. Sci. Instrum. **82**(3), 034902-1–034902-6 (2011)

24. Yang, J., Silvestro, C., Khatri, D., De Nardo, L., Daraio, C.: Interaction of highly nonlinear solitary waves with linear elastic media. Phys. Rev. E **83**(4), 046606-1–046606-12 (2011)

25. Yang, J., Dunatunga, S., Daraio, C.: Amplitude-dependent attenuation of compressive waves in curved granular crystals constrained by elastic guides. Acta Mech. **223**(3), 549–562 (2012)

26. Yang, J., Silvestro, C., Sangiorgio, S.N., Borkowski, S.L., Ebramzadeh, E., De Nardo, L., Daraio, C.: Nondestructive evaluation of orthopaedic implant stability in THA using highly nonlinear solitary waves. Smart Mater. Struct. **21**, 012002-1–012002-10 (2012)

27. Yang, J., Sangiorgio, S.N., Borkowski, S.L., Silvestro, C., De Nardo, L., Daraio, C., Ebramzadeh, E.: Site-specific quantification of bone quality using highly nonlinear solitary waves. J. Biomech. Eng. **134**, 101001-1–101001-8 (2012)

28. Ni, X., Rizzo, P.: Use of highly nonlinear solitary waves in NDT. Mater. Eval. **70**, 561–569 (2012)

29. Ni, X., Rizzo, P., Yang, J., Katri, D., Daraio, C.: Monitoring the hydration of cement using highly nonlinear solitary waves. NDT E Int. **52**, 76–85 (2012)

30. Ni, X., Rizzo, P.: Highly nonlinear solitary waves for the inspection of adhesive joints. Exp. Mech. **52**(9), 1493–1501 (2012)

31. Johnson, K.L.: Contact Mechanics. Cambridge University Press, Cambridge (1985)

32. Tsuji, Y., Tanaka, T., Ishida, T.: Lagrangian numerical simulation of plug flow of cohesionless particles in a horizontal pipe. Powder Technol. **71**(3), 239–250 (1992)

33. Hunter, S.C.: Energy absorbed by elastic waves during impact. J. Mech. Phys. Solids **5**(3), 162–171 (1957)

34. Kuwabara, G., Kono, K.: Restitution coefficient in a collision between two spheres. Jpn. J. Appl. Phys. **26**, 1230–1233 (1987)